Geophys. J. Int. (2009) **177,** 1256–1264 doi: 10.1111/j.1365-246X.2009.04110.x

Seismic shear wave splitting in upper crust characterized by Taiwan tectonic convergence

Emmy T. Y. Chang,[1] Wen-Tzong Liang[2] and Yi-Ben Tsai[3]

[1] *Institute of Oceanography, National Taiwan University, Taipei, Taiwan. E-mail: etychang@ntu.edu.tw*
[2] *Institute of earth Sciences, Academia Sinica, Taipei, Taiwan*
[3] *Pacific Gas and Electric Company, San Francisco,* CA 94105, *USA*

Accepted 2008 December 19. Received 2008 December 18; in original form 2008 August 14.

SUMMARY

This study conducts a comprehensive investigation of crustal seismic anisotropy over varied geological regimes of Taiwan. With a large amount of earthquake data, the lateral variation of seismic shear wave splitting (SWS) is fully examined in terms of crustal deformation process. As the well-known vigorous orogeny subjected to the Eurasian–Philippine plate collision, tectonic convergence of Taiwan is presumably propagating from east to west. The acquired SWS waveform data cover areas from the slightly deformed Western Plains to the intermediate-to-high metamorphic Western Foothills and central mountain ranges. By means of waveform cross-correlation, the SWS parameters—the fast-wave polarization orientation and delay time—infer that the mechanism of lithologic deformation of Taiwan convergence can be classified into two domains: the convergence-parallel laminating west of the Deformation Front and the convergence-perpendicular striking east of the Deformation Front. The convergence-parallel SWS measurement presents the internal fabrics consisting of microfractures subject to lateral compression before the yielding of the lithologic strength, whereas the convergence-perpendicular measurements reveal the lateral accommodation of deformation as the stress/strain surpass the yielding strength of rock, where the predominant SWS polarization is in the NE–SW direction similar to the general trend of Taiwan's mountain ranges. It is remarkable that there is no correlation between metamorphic degrees with SWS parameters. The geological province which corresponds to higher metamorphism is not consistent with large SWS parameters. This may be because of anisotropic weakness caused by multiple tectonic processes at considerable metamorphic zone. Furthermore, comparison of the SWS delay times with corresponding focal depths suggests that seismic anisotropy in the upper crust may come from multiple layers, and the fabric lamination causing the anisotropy may be confined only within the shallow crust.

Key words: Microstructure; Seismic anisotropy; Fractures and faults.

1 INTRODUCTION

Analogous to optical birefringence, seismic shear waves (or *S* waves) travel in an anisotropic media with velocities dependent on the propagation and polarization directions, in particular, characterized by shear waves polarized in one specific direction travelling faster than those polarized in the orthogonal direction (e.g. Ando *et al.* 1983; Crampin 1984; Bowman & Ando 1987). Conventionally, such a seismic anisotropy physically originates from lithologic matrix alignment or structural fabrics caused by tectonic stresses. A fast shear wave vibrates in a specific polarization and a time delay appears between the first and subsequent arriving phases of the direct *S* waves, known as the seismic shear wave splitting (SWS) phenomenon. Thus, the fast polarization direction (ϕ) and the time delay (Δt) have become two recognized SWS parameters, commonly used to specify the stress regime in the media and to construct the relationship between lithologic deformation and tectonic forces.

Recent applications of measuring SWS can be set into two motifs respectively corresponding to teleseismic and local/regional observation. Adoption of the teleseismic waveforms of *S*, *ScS*, *SKS*, etc. tends to resolve the influence of material flow within the upper mantle. In that case, the typical determinations for the magnitude of SWS delay time are in the range of 0–2 s (e.g. Mainprice & Silver 1993; Gledhill & Gubbins 1996; Kendall & Silver 1996; van der Lee & Nolet 1997; Fouch *et al.* 2000; Rau *et al.* 2000). These studies draw a feature for SWS polarization mainly perpendicular to the tectonic forces as a ductile flow subject to convergence. In contrast to the mantle-flow-induced polarization, the SWS in

shallow layers reflects complex brittle deformation and raises attention to faulting behaviour within the rocks. Up to date, lots of discussions have been laid on the anisotropy models in terms of rock cracks and fractures (e.g. Hudson 1981, 1994; Schoenberg & Douma 1988; Vavryčuk 1993). Some current studies depicted that the propagation of seismic waves may be parallel to layer foliation or lithologic fibre, whereas the anisotropy density would vary in proportion to the pressure or metamorphic grade (Okaya *et al.* 1995; Godfrey *et al.* 2000; Meltzer & Christensen 2001). Influences of fluid injection and generation of microcracks were also introduced to explain the different orientations w.r.t. local stress field (Crampin 1984; Crampin *et al.* 1985). Further on this subject, the appearance of fracture healing during earthquake cycle along the specific fault is considered by many authors (e.g. Li *et al.* 1998; Tadokoro *et al.* 1999, 2002; Tadokoro & Ando 2002), but did not overwhelmingly approved by every local SWS observation (Zinke & Zobak 2000; Liu *et al.* 2004).

It is evident that there still lacks a comprehensive observation over varied geological regimes to compose a distinct image for the seismic anisotropy in the upper crust. In this study, we focus on the convergent lithologic stain in the upper crust based on the upper crust earthquakes at Taiwan. Taiwan island is well known to subject to a tectonic convergence and therefore a vigorous lithospheric orogeny and deformation along the western boundary of the Pacific Rim (e.g. Suppe 1984; Angelier 1986; Ho 1986; Wu *et al.* 1997). Seismic data adopted in this paper are from the island-wide dense accelerometric network. The SWS parameters, including the fast direction of polarization and delay time between fast and slow shear waves, are determined for each earthquake record by a waveform cross-correlation method. With a large amount of earthquake data, we demonstrate directly the relationship of the seismic anisotropy with the shallow geology, especially to examine the seismic anisotropy and the metamorphic degrees. Factors causing the complexity of upper crustal anisotropy are discussed in this paper. It also shows that deformation fabrics in the upper crust can be varied in a very short range. Different to the consequence of individual lithologic experiments, we first provide a full image for the directional consistency between crustal SWS characteristics and local strain.

Previous studies on seismic anisotropy of Taiwan focused mainly on tectonic influence in the lower crust and upper mantle (e.g. Rau *et al.* 2000; Huang *et al.* 2006). These trend studies showed consistent orientations of fast-wave polarization, suggesting strong correlation between Taiwan's orogeny and upper mantle deformation. In general, the orientations of anisotropy for the upper mantle and lower crust are parallel to Taiwan's mountain ranges, but perpendicular to the direction of plate convergence. Jointly with the results for the deep layers of lithosphere, we report here a new aspect for the shear wave anisotropy as well as the possible relationship between the anisotropy and microstructures within the orogenic process.

2 UPPER CRUST GEOLOGICAL SETTINGS OF TAIWAN

The island of Taiwan is located at the boundary between the colliding Pacific and Eurasian plates. In the eastern offshore Taiwan, the Philippine plate subducts beneath the Eurasian plate while simultaneously upducting upon the Eurasian plate along the Longitudinal Valley (Fig. 1a). This has caused an oblique collision and a series of orogenic deformation in Taiwan since 2 Ma (Tsai 1978; Suppe 1981; Ho 1986). In terms of the shallow deformation, the most notable manifestation is surface topography, in the form of either gradual ascending/descending relief laid on crustal faulting/folding or abrupt mountain building. Subject to the NW–SE convergent force, the mountain ranges in central Taiwan are roughly parallel to each other in the NE–SW direction, which is essentially orthogonal to the direction of principal convergence stress. Major faultings with an important thrusting component are aligned in the same direction. In the meantime, considerable lateral movements take place along these faults, especially at the Longitudinal Valley, due to oblique convergence of the plates (Ho 1986). The trajectories of the maximum tectonic strain (ε_1, red lines in Fig. 1a) derived from the displacement field based on data from campaigns and continuous GPS measurements show a main NW–SE shortening in the plate convergence direction throughout the Taiwan island (Yu *et al.* 1997; Chang *et al.* 2003) (Fig. 1). A directional change in strain trajectories is merely seen at the northeastern end of the Taiwan island—the Ilan Plain, which is reported as a pull-apart alluvial sedimentary basin tectonically dominated by a strike-slip deformation mechanism for the current stage (Chang *et al.* 2003; Angelier *et al.* 2009) (Fig. 1).

Typically, the distinct shallow geology corresponding to Taiwan convergence provides background information for further discussion of tectonic stress/strain regime. Apart from the eastern Coastal Range, which is situated at the collision suture zone and identified as parts of the Philippine Plate, the main geological provinces of Taiwan are divided by geological identifications and significant mega-thrusts (Ho 1986; Chang *et al.* 2001). They are, from east to west, the Backbone Range (BRB)—mostly greenshist-grade metamorphic rocks with some gneiss, the Hsuëshan Range (HSR)–interleaved meta-sandstones and slates/argillites, the Western Foothill belt—compacted sandstones and siltstones, and finally the Western Plains—unconsolidated Holocene sediments (Fig. 1b). It is considered that the microstructures responding to local lithologic stress are simultaneously generated with different deforming stages (Ho 1986). The Taiwan orogenic model conventionally sets the crustal deformation beginning at the Longitudinal Valley and propagating westward towards the Western Plains, and the diminution of the topography (the EW profile T-T′ in Fig. 1) as well as the decreasing metamorphic grades from east to west across Taiwan. The Western Foothills and the Western Plains are considered to stay at the initial or light orogenic stages (Chen *et al.* 1983; Ho 1986) (Fig. 1). An apparent topographic feature that conjoins the topographic slope to the zero elevation level separating the Foothills belt and the Western Plains is denoted as the Deformation Front. Even though the whole Taiwan area is affected by the plate convergent force, the areas to the west of the Deformation Front show no specific ground deformation from the series of folding and mountain building. However it is generally considered that the surface trace of the Deformation Front gradually moves towards the west with the propagating orogeny (e.g. Suppe 1981; Ho 1986; Chang *et al.* 2001).

3 SEISMIC DATA AND SWS MEASUREMENTS

We use the seismic records acquired from the dense free-field three-component accelerometer network, which is deployed by Taiwan's Central Weather Bureau in populated areas as part of the Taiwan Strong Motion Instrumentation Program (TSMIP) for the purpose of providing much needed data for seismic hazard mitigation and earthquake research (Shin *et al.* 2000). One of the densest in the

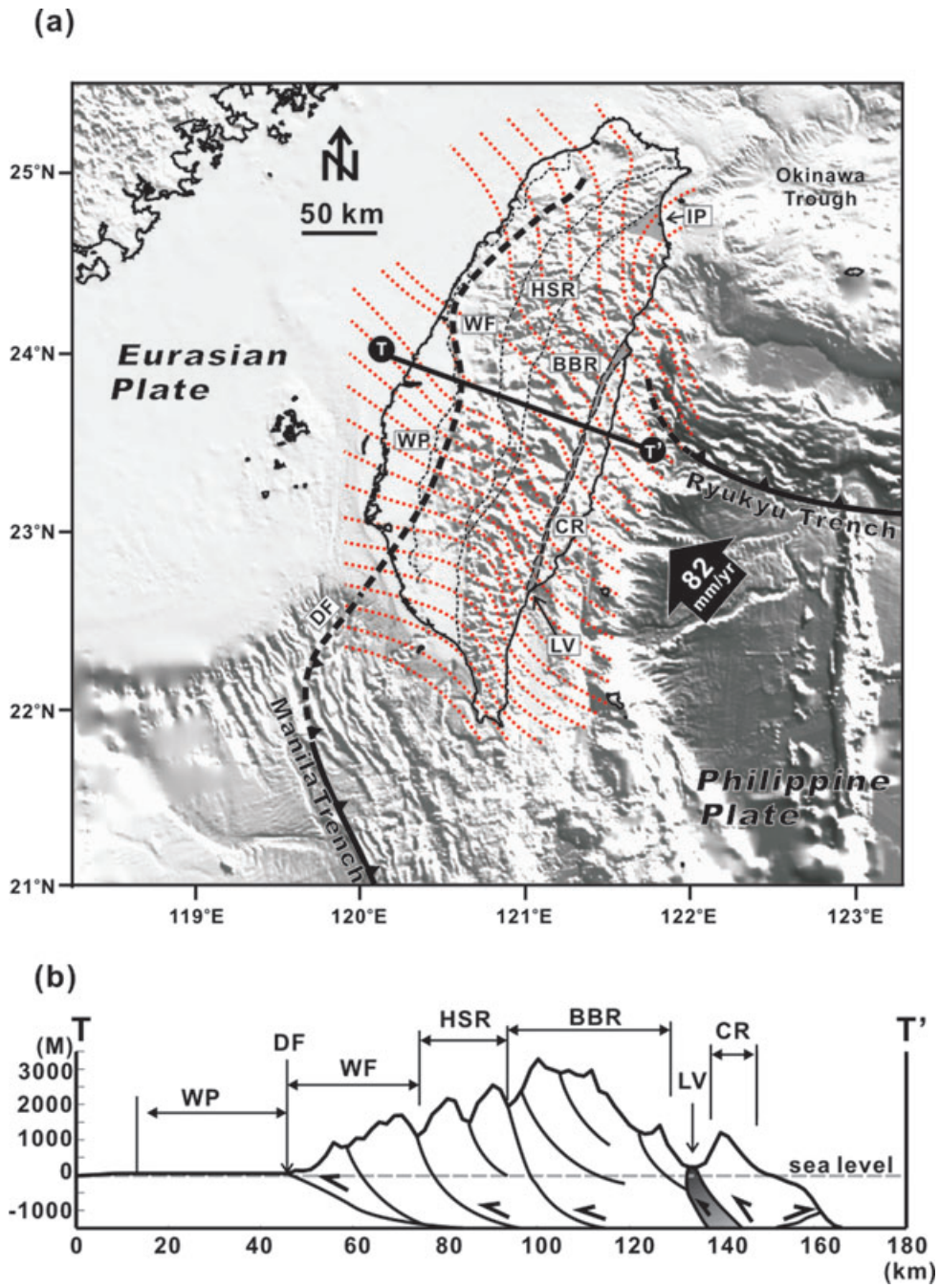

Figure 1. (a) Geological framework around Taiwan. Displacement of the Philippines Sea plate relative to the Eurasia plate is indicated by the large black arrow at the lower-right corner with velocity according to GPS studies (Yu *et al.* 1997). Abbreviated terms of tectonic units are as follows: BBR, Backbone Range; CR, Coastal Range; DF, Deformation Front; HSR, Hsuëshan Range; IP, Ilan Plain; LV, Longitudinal Valley; WP, Western Plain. Red dash lines show the maximum stress trajectories, as adopted from Chang *et al.* (2003). (b) The T-T′ profile across varied tectonic units, as indicated in plan trace in (a), illustrating a westernward thrusting sequence of deformation in Taiwan convergent tectonic regime. Here topographic elevation adopted from the Taiwan DEM model (ref); illustration of geological structure is modified from Ho (1986) and Chang *et al.* (2001).

world, TSMIP presently has more than 700 free-field stations covering every 3 × 3 km in the metropolitan areas. The TSMIP accelerometers have a flat response over frequencies ranging from DC to 50 Hz. They are operated in trigger mode with a 20-s pre-event memory and will record additional 5 s after the signal falls below a preset threshold (∼ 3.92 gal). Ground motion signals are typically digitized at 200 samples per second with a 16-bit resolution. Since 1995, the TSMIP network has recorded not only strong ground motions of many large earthquakes, but also moderate ground motions from numerous small, local events. This study uses mainly the latter type of data.

We selected appropriate records from 1995 to 2003 in the TSMIP database. Since our goal is to study SWS features in the upper crust, events deeper than 40 km are excluded. To avoid complexity of converted phases due to reflection/refraction between layers, the incident angle is limited to within 35°, so that the ray paths basically

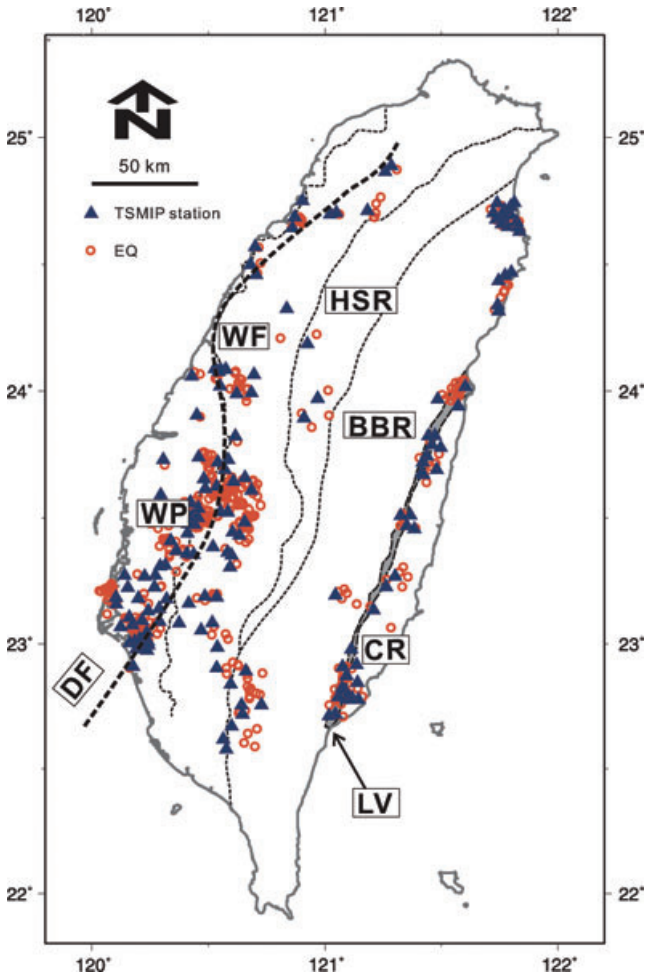

Figure 2. Spatial distribution of the epicentres of selected events (red open circle) and recording stations (blue triangle). They cover almost all major geological provinces.

travel vertically. Only clean *S*-wave impulses with a signal-to-noise (S/N) ratio greater than 3.0 are acceptable. Thus, the selected records are mostly simple and clean from small earthquakes located close to the recording stations. To prevent complication of source effects on signals, we screen out the larger events by imposing a magnitude threshold of smaller than 3.5. These events are in magnitude ranging from 2.0 to 3.5 (M_L).

The spatial distribution of the used TSMIP stations (in triangle) and earthquakes (in red dot) is shown in Fig 2. In total, 464 SWS measurements were made in this study. Except the high mountain areas, our dataset covers the whole major geologic provinces of Taiwan, from the intermediate-to-high metamorphic zones in eastern Taiwan (i.e., HSR and BBR) to the slightly deforming Western Plains. The majority of these events are shallower than 20 km.

Each record (of ground acceleration) is integrated twice to get the displacement waveform, and bandpass filtered between 0.01 and 10 Hz, corresponding to the spectra of direct *S* waves for small-to-moderate earthquakes. Fig. 3 shows examples of SWS recorded at some stations. In general, the splitting of fast and slow phases can be visually identified on horizontal seismograms. Arrival offsets of 0.1–0.3 s between the fast and slow *S* phases can be visually estimated. Their particle motions show that the early arrivals of fast waves are vibrating almost perpendicularly to the later arrivals of slow waves (Fig. 3).

For robustness, we use a waveform cross-correlation method to determine the best values of the SWS parameters (ϕ, Δt) for each record. A *t*-test of cross-correlation coefficient is adopted to determine the 95 per cent confidence limit of estimation and to assess the reliability of analysis. Fig. 4 shows a sample plot of varying cross-correlation coefficient with (ϕ, Δt). In this case, a pair of the SWS parameters (−72, 0.165) would give the best solution. Its 95 per cent confidence limits are marked in bold dash lines and can be read within ±15° for fast-wave polarization azimuth and ±0.01 s for delay time estimation, respectively.

We simultaneously count the traveltimes of direct *S* waves from each seismic source, the *S*-wave velocities can be determined from the traveltime and the length of travel path. The shear-wave velocity variance of each event–station pair can compose the local anisotropy index as calculated by $(V_{fast} - V_{slow})/V_{ave}$, where V_{fast} and V_{slow} are the velocities of the fast and slow shear waves and V_{ave} is the average velocity (e.g. Wang *et al.* 1989; Okaya *et al.* 1995). Technically, this index represents the averaged anisotropy degree along the seismic travel path.

4 SPATIAL FEATURES OF SWS PARAMETERS

Fig. 5(a) shows a map of the measured SWS polarization orientation and delay time, as plotted at the midpoint between each event's epicentre and its recording station. Also shown is the Deformation Front (in thick dash lines) and trajectories of the maximum compression stress (in dotted lines). Note that the most distinct seismic anisotropy is observed in the Western Plains, which is undergoing an initial stage of lithologic deformation in Taiwan's orogenic process (Suppe 1981; Ho 1986). This observation varies from the model of increasing of the anisotropy degree with the augmentation of lithologic metamorphism (Chen *et al.* 1983; Ho 1986; Ernst & Jahn 1987). Furthermore, drastic changes in both SWS parameters, that is, the fast-wave polarization direction and delay time, are observed across the Deformation Front separating the Western Plain and Western foothills.

This result shows that the Deformation Front is an important boundary for seismic anisotropy development within the upper crust. It is observed that the SWS polarizations are mostly parallel to the maximum compression stress west of the Deformation Front line and perpendicular to the maximum compression stress east of the Deformation Front line, the latter case are parallel to the general trends of the HSR and BBR. This raises to consider that the orientation of SWS polarization submits to principal compressional strain (ε_1) before the distinct deformation occurs with the stressed rock, whereas it turns to follow the direction of the elongation strain (ε_3) as the accumulated tectonic stress overcomes the yield stress and the orientation of SWS polarization parallel to fold crest, fault strike or newly generated. Some experiments conducted in laboratory have confirmed that the SWS polarization will follow the mineral alignment of the schist (e.g. Godfrey *et al.* 2000). One thing worth mentioned here is that the measurement of SWS delay times also shows a distinct change at the Deformation Front; the ones taken in the west areas of the Deformation Front line are larger than those in the east areas.

Fig. 5(b) shows the velocity anisotropy index determined from shear-wave velocity variance of each event–station pair. Not similar to the distribution of SWS parameters, the velocity anisotropy at the upper crust reveals no correlation with the geological regimes. The maximum anisotropy of 16 per cent is observed in the Western

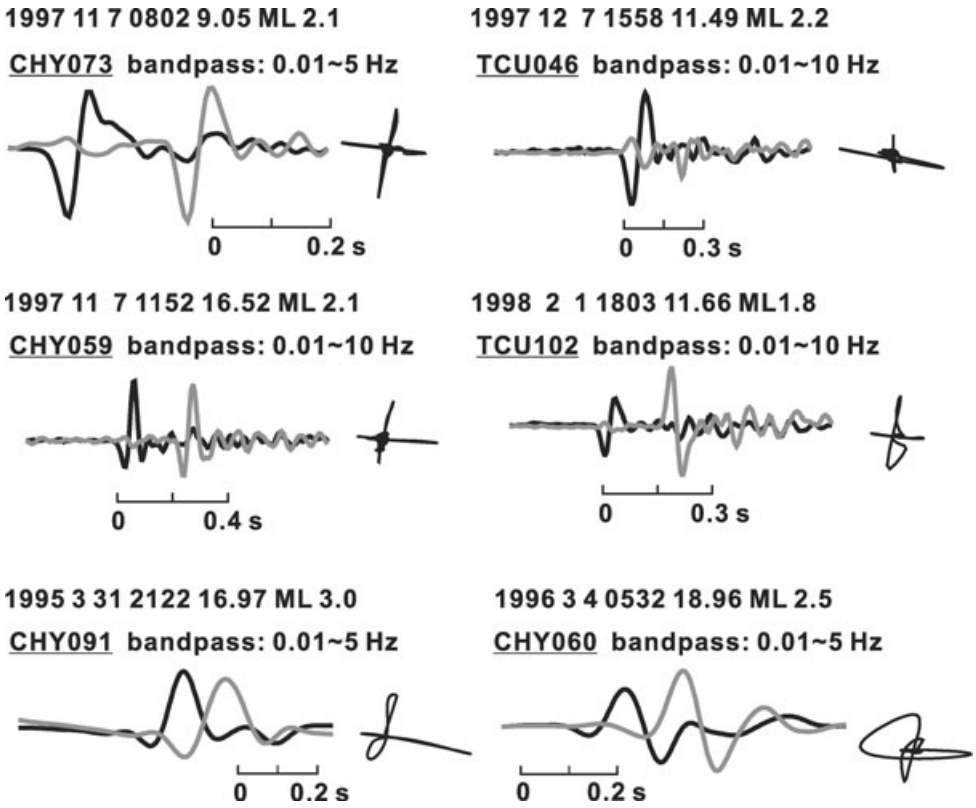

Figure 3. Examples of SWS waveforms. Particle motions exhibit a clear cross vibration for fast and slow shear waves. The head line above each subfigure indicates the origin time, magnitude (ML) and station.

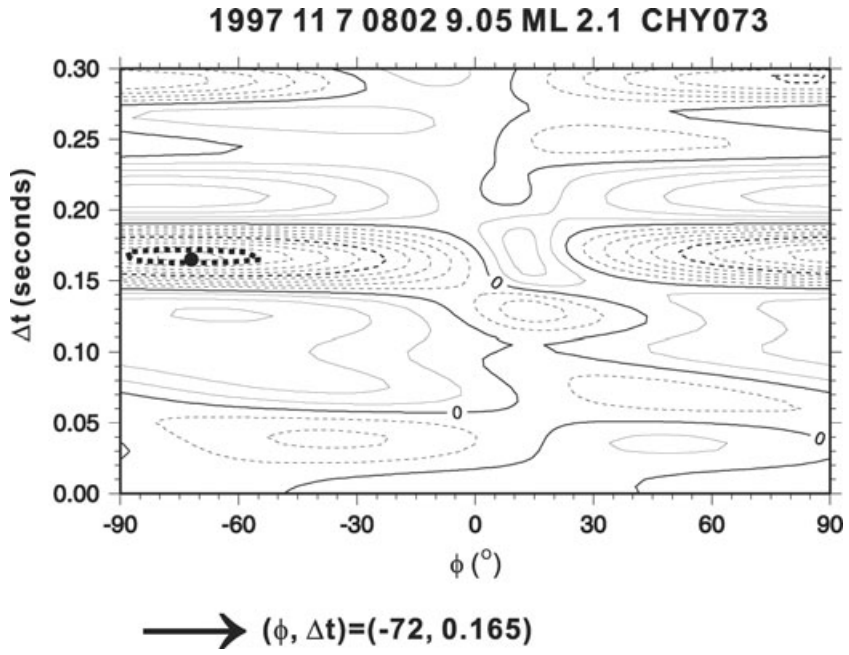

Figure 4. Plot of correlation coefficient as function of ϕ and Δt. The best estimation is denoted by the black solid dot; the black bold dash line indicates the area of 95 per cent confidence level.

foothills. Except a few clusters of high anisotropy, most measurements yield anisotropy below 6 per cent. This shows that the large anisotropy may merely consist with the locally high deformation within rock in the upper crust. Further discussions about the velocity anisotropy are depicted in the following context.

5 DISCUSSIONS

5.1 Multiple layers for SWS in the upper crust

Fig. 6 plots the Δt versus corresponding P–S traveltime difference, T_{PS}, for each event. T_{PS}, as measured from P- and S-arrival phases

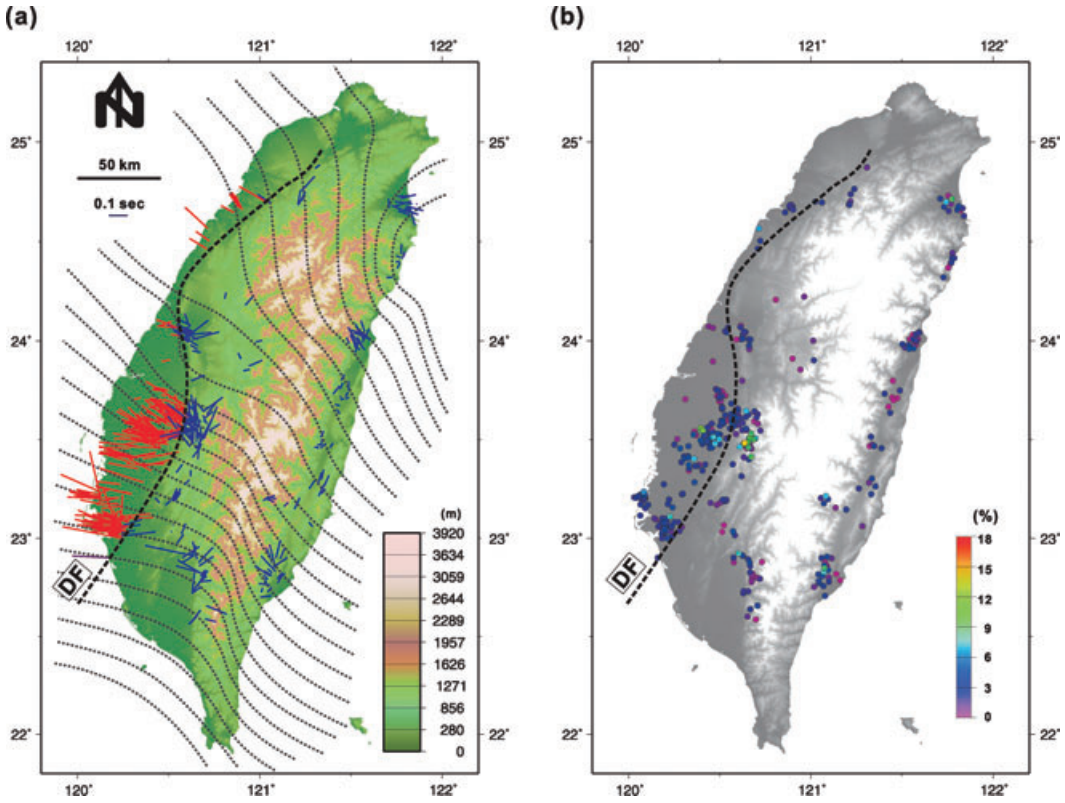

Figure 5. (a) Plots of the measured SWS parameters. Fast-polarization direction and delay time are represented by azimuth and length of bar. Black dash lines show the maximum stress trajectories (Chang *et al.* 2003). (b) Spatial distribution of anisotropy estimation.

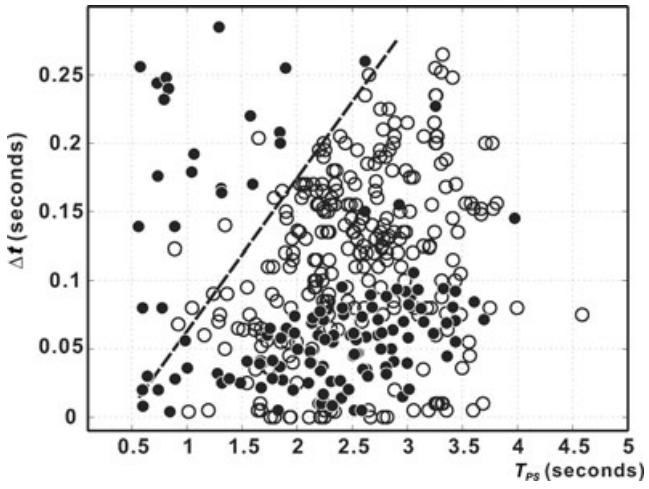

Figure 6. Plot of the observed delay time (Δt) versus *P*–*S* traveltime differences (T_{PS}). Bold dash line indicates an approximate positive proportion between Δt and T_{PS}. Open and close dots represent the measurements observed from areas west and east of the Deformation Front, respectively.

on seismograms, is proportional to the length of travel path. Ideally, if the lithologic layer is homogeneous, Δt would fit a linear trend with increasing T_{PS}, that is, increasing travel path. Fig. 6 shows a roughly positive relationship between Δt and T_{PS}, yet they do not exactly fit a linear function. The bold dash line in Fig. 6 illustrates the inference of their linear positive correlation. It is remarkable that the majority of T_{PS}–Δt plots are on the right-hand side of this reference line. In fact, T_{PS} shows diffused patterns for a specific Δt, and vice versa. The upper crust in Taiwan appears inhomogeneous in terms of the SWS characteristics, and the anisotropy degree cannot be determined by simply incorporating the factors of the thickness of the anisotropic layer and a unique SWS density per volume. In other terms, the source layer of seismic anisotropy may be multiple and vary for different SWS measurement. This may be the cause of crustal seismic anisotropy, as the values of the SWS parameter relate to the factors of seismic velocity, travel path, and anisotropy amount. Some SWS observations also reported that the irregular topography may be a factor that causes a scattering of SWS patterns (Gao & Crampin 2006; Gao *et al.* 2008). Fine structural fabrics may be variously constructed according to local structures, for instance, fault zone, specific lamination within an identical lithology and different topographic developments. To shed light on the source of seismic anisotropy in the upper crust awaits more detailed survey.

Figs 7(a) and (b) show the histograms of the SWS delay time (Δt) and azimuth of fast-wave polarization (ϕ), respectively. It shows bimodal distributions both for the delay time and fast-wave polarization. This suggests the presence of two distinct groups of SWS characteristics for the upper crust of Taiwan. In view of Fig. 5(a) and 7(a) further shows the ranges of Δt for the two groups, peaking around 0.05 and 0.15 s, respectively. The first group (blue curve) includes mostly the data points observed in the central mountains (HSR, BBR) and Western Foothills, whereas the second group (red curve) includes mainly measurements in the Western Plains. Similarly, Fig. 7(b) shows two distinct ranges in the observed ϕ: one centred around 40° and the other around 100°. The former group mostly appears in the high mountain areas and Western Foothills, whereas the latter group mainly in the Western Plains.

The average velocity of direct *S* wave for the layers shallower than 20 km in the Western Plains is determined to be 3.0 km s^{-1} (e.g. Chen 1995; Shih *et al.* 1998). Taking into consideration this V_{ave} and

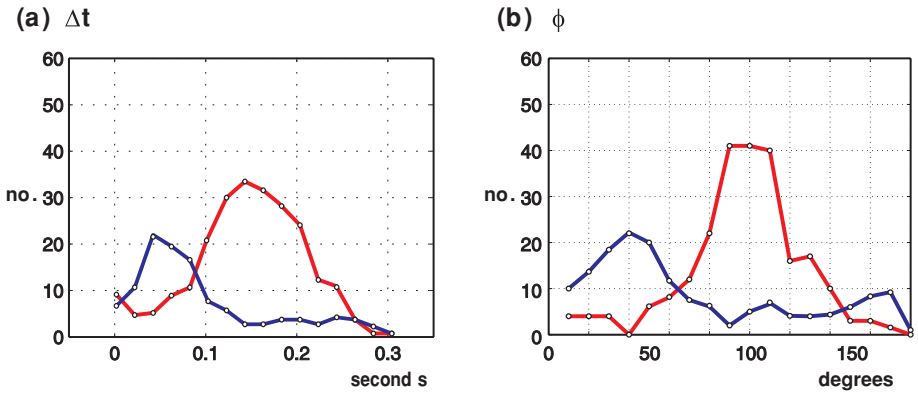

Figure 7. Histograms of (a) delay time and (b) fast-wave polarization orientation. Red and blue curves represent the measurements obtained for the areas west and east of the Deformation Front, respectively.

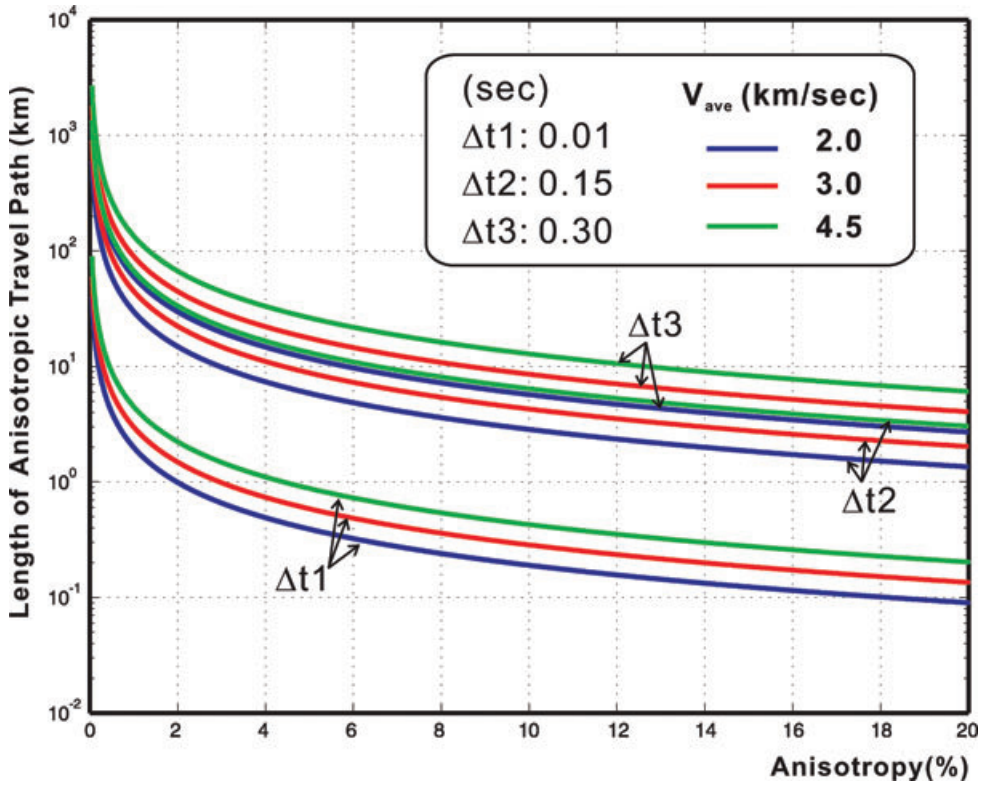

Figure 8. Plots of anisotropy percentage versus length of anisotropic travel path. Various conditions in seismic velocity and delay time are indicated in the plot.

a delay time of 0.15 s, the theoretical length of anisotropic travel path would be about 10–15 km with respect to 3–6 per cent anisotropy. This is roughly consistent with the observations in the Western Plains of Taiwan (where the focal depth of events is around 10–15 km and the anisotropy amount is on the same order). Fig. 8 shows the length of the anisotropic path as a function of seismic anisotropy amount (from 0 to 20 per cent) at given V_{ave} (2.0, 3.0 and 4.5 km s^{-1}) and delay time (0.01, 0.15 and 0.3 s). It illustrates that higher anisotropy corresponds to a shorter anisotropic travel path with respect to the specific delay time or V_{ave}. Given a specific anisotropy index and a fixed length of anisotropic travelling path, one can get different delay times at various shear wave velocities. This means that local heterogeneity in velocity may play an important role in determining the SWS. On the contrary, a given delay time is the result of integrating various factors of seismic velocity, travel path and anisotropy degree. Considering that the focal depths of events used in this study are mostly deeper than 5 km, the high anisotropy and small anisotropic travel path in Fig. 8 (say 16 per cent and around 0.3 km) reveal that seismic anisotropy may reflect from merely some layers within the crust.

5.2 Relationship between SWS parameters and tectonic strain

In Fig. 5(a), large delay times appear in the Western Plains with a maximum value reaching around 0.3 s. Although almost all part of Taiwan is subjected to the NW–SE convergence, the fast-wave polarization east of the Deformation Front shows a conspicuous

alignment perpendicular to the NW–SE convergence. Instead, it is parallel to the general NE–SW trend of mountain ranges. One can further infer in this case that the development of structural fabrics mainly subjects to the lateral deformation in areas of active orogeny, as convergent stress surpasses the yielding strength of rock. In contrast, the SWS measurements in the Western Plains west of the Deformation Front suggest that the fabric lineation aligns with the orientation of maximum stress before the onset of significant orogeny. Such a feature may be due to lithologic fragments in a fine-grained foliated matrix of phyllosilicates, or to microcracks or small fissures within rocks at the initiation of strata deformation in convergent regime.

Another important observation for SWS measurement is that the delay times in the areas east of the Deformation Front are significantly smaller than the western areas, differing by a factor of more than 2. It is often thought that the higher metamorphism would create stronger lithologic foliations, thus resulting in greater shear wave anisotropy. However, the shallow crustal layers have a quasi-free boundary in the vertical direction. The shallow structural fabrics generated from lateral compression forces are the result of lithologic texture in accommodation to many local factors (e.g. tectonic forces, overburden loading and mineral composition, etc.). Fossil cracks or alignments generated by previous tectonic processes may remain in the strata instead of being totally erased by subsequent processes. The structural lamination generated in various orogenic stages might be in different orientations. Their overlay can weaken the overall birefringence effect, resulting in neutralization of seismic anisotropy and smaller delay times ($<$0.1 s), even in areas further to the east of the Western Foothills in the well-developed central mountain ranges with high lithologic metamorphism.

Limited by the TSMIP network coverage, only a few SWS were measured in central Taiwan. Our SWS analysis thus cannot further distinguish between the Western Foothills and the eastern metamorphic areas. On the other hand, the similarity in the observed SWS features between these two regions suggests that there may not be significant anisotropic enhancement with increasing metamorphic grade in Taiwan.

5.3 Distinct SWS characteristics in the upper crust and greater depths

Several previous studies using teleseismic *S*, *ScS* and *SKS* phases have determined the SWS parameters to characterize seismic anisotropy of the lower crust and upper mantle beneath Taiwan (e.g. Kuo *et al.* 1994; Rau *et al.* 2000; Huang *et al.* 2006). These trend studies showed consistent orientations of fast-wave polarization, suggesting strong correlation between Taiwan's orogeny and upper mantle deformation. In general, the orientations of anisotropy for the upper mantle and lower crust are parallel to Taiwan's mountain ranges, but perpendicular to the direction of plate convergence. However, estimations of SWS delay time have a large variance of more than 1.0 s among these analyses. Huang *et al.* (2006) attributed these relatively large discrepancies to source side-effects or different frequency bands adopted in these studies.

In comparison with the SWS parameters observed previously from longer period *S* phases, that is, *SKS* or *ScS*, and on deeper deformation, the fast-wave polarization of our study is generally consistent with their results in the mountain areas, but shows distinct variations in the Western Plains. This study resolves lithologic fabric alignment in smaller scales, which tend to be sensitive to shallow tectonic forces and may present more random properties. This suggests different mechanisms for lithologic deformation between the upper and lower crust. At high *P*–*T* condition, large viscosity will dominate lithologic deformation in an elastic-to-plastic mode, resulting in alignment of rock deformation with major structural trends (Deffontaines *et al.* 1994; Shyu *et al.* 2005). Our finding of the general alignment of fast-wave polarization in the upper crust with the trend of mountain ranges suggests that under high mountain elevations tectonic forces have overcome lithologic strength to cause sequences of plastic deformation. However, we should note here that the deformation in the shallow mountain areas is not totally plastic; much of the internal alignments are not always consistent with the ones associated with the orogeny. Consequently, no large SWS parameters are determined in the shallow mountain areas.

Contrary to the general alignment of SWS polarization with main mountain ranges, orientations of the fast-wave polarization in the Western Plains are parallel to the direction of plate convergence. This can be interpreted as initiation of fabric alignment within the rocks. The 90° change in polarization direction from the Western Plains to the central mountain areas, as found in this study, indicates a change of lithologic deformation from brittle elastic mode to plastic flow mode. This inference can partially support the lithospherical bulking of Taiwan's orogeny. Once mountain building commenced, the strata deformed in plastic-like mode over large lithospheric scales.

6 CONCLUSIONS

We have made a systematic study of the SWS parameters for the upper crust of Taiwan. In terms of tectonic deformation, we find that the SWS characteristics in upper crust can be classified in two domains: (1) west of the Deformation Front, convergence-parallel structural lamination dominates. Here we see the fabrics align in the NW–SE direction where microtextures are initiated by lateral forces; (2) east of the Deformation Front, development of lithologic fabrics mainly conforms to the general NE–SW trend of convergence-perpendicular orogeny with smaller delay times.

Aligned microstructures, such as visible fractures or mineral lamination, are often considered as the primary mechanism for generating the SWS phenomenon in shallow crust. This hypothesis may need to be modified to allow for the presence of heterogeneity in material ingredients. Furthermore, the SWS characteristics observed in the upper crust under mountain areas are compatible with the results of previous studies for greater depths. They appear to share similar plastic deformation patterns parallel to the general trend of the central mountain ranges. On the contrary, the SWS characteristics in the shallow crust of the Western Plains are of brittle elastic deformation mode. This suggests that deformation in the upper crust in Taiwan may be laterally discontinuous and viscosity may vary as a function of orogenic stages.

ACKNOWLEDGMENTS

This study stems from the iSTEP multidisciplinary project supported by the Ministry of Education and the National Science Council of Taiwan in two phases. We thank Miss Mei-Yu Chen for assistance in data processing and two anonymous reviewers and the Editor for improving this paper. This study has made use of the CWB TSMIP database and the GMT graphics software.

REFERENCES

Ando, M., Ishikawa, Y. & Yamazaki, F., 1983. Shear wave polarization anisotropy in the upper mantle beneath Honshu, Japan, *J. geophys. Res.,* **88,** 5850–5864.

Angelier, J., 1986. Geodynamics of the Eurasia-Philippine Sea plate boundary: preface, *Tectonophysics,* **125,** IX–X.

Angelier, J. *et al*. 2009. Does extrusion occurs at both tips of the Taiwan collision belt? Insights from active deformation studies in the Ilan Plain and Pingtung Plain regions, *Tectonophysics,* **466,** 356–376.

Bowman, J.R. & Ando, M., 1987. Shear-wave splitting in the upper mantle wedge above the Tonga subduction zone. *Geophys. J. R. astr. Soc.,* **88,** 25–41.

Chang, C.P., Angelier, J., Huang, C.Y. & Liu, C.S., 2001. Structure evolution and significance of a mélange in a collision belt: the Lichi Mélange and the Taiwan arc-continent collision. *Geol. Mag.* **139,** 633–651.

Chang, C.P., Chang, T.Y., Angelier, J., Kao, H., Lee, J.C. & Yu, S.B., 2003. Stress and strain field in Taiwan oblique convergent system: constrains from GPS observations and tectonic data. *Earth planet. Soc. Lett.,* **214,** 115–127.

Chen, Y.L., 1995. Three Dimensional Velocity Structure and Kinematic Analysis (in Chinese with English Abstract), Master dissertation, National Central University, Chungli, pp. 172.

Chen, C.H., Chu, H.T., Liou, J.G. & Ernst, W.G., 1983. *Explanatory Notes for the Metamorphic Facies Map of Taiwan,*Vol. 2, pp. 1–32, Centl Geol. Surv., Special Publication.

Crampin, S., 1984. Effective anisotropic elastic constants for wave propagation through cracked solids, *Geophys. J. R. astr. Soc.,* **76,** 135–145

Crampin, S., Booth, D.C. & Ucer, S.B., 1985. Shear-wave polarizations near north Anatolian fault, evidence for anisotropy-induced shear wave splitting, *Geophys. J. R. astr. Soc.,* **83,** 61–73.

Deffontaines, B., Lee, J.C., Angelier, J., Carvalho, J. & Rudant, J.P., 1994. New geomorphic data on the active Taiwan orogen: a multisource approach, *J. geophys. Res.,* **99,** 20243–20266.

Ernst, W.G. & Jahn, B.M., 1987. Crustal accretion and metamorphism in Taiwan, a post-palaeozoic mobile belt, *Phil. Trans. R. Soc. Lond., A (Math. Phys. Sci.),* **321,** 129–161

Fouch, M.J., Fischer, K.M., Parmentier, E.M., Wysession, M.E. & Clarke, T.J., 2000. Shear wave splitting, continental keels, and patterns of mantle flow, *J. geophys. Res.,* **105,** 6255–6276.

Gao, Y. & Crampin, S., 2006. A stress-forecast earthquake (with hindsight), where migration of source earthquakes causes anomalies in shear-wave polarization, *Tectonophysics,* **426,** 253–262.

Gao, Y., Wu, J., Cai, J.A., Shi, Y.T., Lin, S., Bao, T. & Li, Z.N., 2008. Shear-wave splitting in the southeast of Cathaysia block, South China. *J. Seism.,* doi:10/1007/s10950–008-9126-y.

Gledhill, K. & Gubbins, D., 1996. SKS splitting and the seismic anisotropy of the mantle beneath the Hikurangi subduction zone. *N Z Phys. Earth planet. Inter.,* **95,** 227–236.

Godfrey, J., Christensen, N.I. & Okaya, D.A., 2000. Anisotropy of schists: contribution of crustal anisotropy to active source seismic experiments and shear wave splitting observations. *J. geophys. Res.,* **105,** 27991–28007.

Ho, C.S., 1986. *An Introduction to the Geology of Taiwan—Explanatory Text of the Geologic Map of Taiwan,* Publication of the Central Geological Survey/The Ministry of Economic Affairs, Taiwan.

Huang, B.S., Huang, W.G., Liang, W.T., Rau, R.J. & Hirata, N., 2006. Anisotropy beneath an active collision orogen of Taiwan: results from across island array observations, *Geophys. Res. Lett.,* **33,** L24302, doi:10.1029/2006GL027844.

Hudson, J.A., 1981. Wave speeds and attenuation of elastic waves in material containing cracks, *Geophys. J. R. astr. Soc.,* **64,** 133–150.

Hudson, J.A., 1994. Overall properties of anisotropic materials containing cracks, *Geophys. J. Int.,* **116,** 279–282.

Kendall, J.M. & Silver, P.G., 1996. Constraints from seismic anisotropy on the nature of the lowermost mantle, *Nature,* **381,** 409–412.

Kuo, B.Y., Chen, C.C. & Shin, T.C., 1994. Split S waveforms observed in northern Taiwan: implications for crustal anisotropy, *Geophys. Res. Lett.,* **21,** 1491–1494.

Li, Y.-G., Vidale, J.E., Aki, K., Xu, F. & Burdette, T., 1998. Evidence of shallow fault zone strengthening after the 1992 *M* 7.5 Landers, California, earthquake, *Science,* **279,** 217–219.

Liu, Y.F., Teng, T.L. & Ben-Zion, Y., 2004. Systematic analysis of shear-wave splitting in the aftershock zone of the 1999 Chi-Chi, Taiwan, earthquake: shallow crustal anisotropy and lack of precursory variations, *Bull. seism. Soc. Am.,* **94,** 2330–2347.

Mainprice, D. & Silver, P., 1993. Constraints on the interpretation of teleseismic SKS observations from Kimberlite nodules from the subcontinental mantle, *Phys. Earth planet. Int.,* **78,** 257–280.

Meltzer, A. & Christensen, N., 2001. Nanga Parbat crustal anisotropy: implications for interpretation of crustal velocity structure and shear-wave splitting, *Geophys. Res. Lett.,* **28,** 2129–2132.

Okaya, D., Christensen, N., Stanley, D. & Stern, T., 1995. Crustal anisotropy in the vicinity of the Alpine Fault Zone, South Island, New Zealand, *N. Z. J. Geol. Geophys.,* **138,** 579–583., *Earth planet. Sci Lett.,* **177,** 177–192.

Rau, R.J., Liang, W.-T., Kao, H. & Huang, B.S., 2000. Shear wave anisotropy beneath the Taiwan orogen. *Earth Planet. Sci Lett.* **177,** 177–192.

Schoenberg, M. & Douma, J., 1988. Elastic wave propagation in media with parallel fractures and aligned cracks, *Geophys. Prospect.,* **36,** 571–590.

Shih, R.C., Lin, C.H., Lai, H.L., Yeh, Y.H., Huang, B.S. & Yen, H.Y., 1998. Preliminary crustal structures across central Taiwan from modeling of the onshore-offshore wide-angle seismic data. *Terr. Atm. Ocean. Sci.,* **9,** 317–328.

Shin, T.C., Kuo, K.W., Lee, W. H. K., Teng, T.L. & Tsai, Y. B., 2000. A preliminary report on the 1999 Chi-Chi (Taiwan) earthquake, *Seism. Res. Lett.,* **71,** 24–30.

Shyu, J.B., Sieh, K., Chen, Y.G. & Liu, C.S., 2005. Neotectonic architecture of Taiwan and its implications for future large earthquakes, *J. geophys. Res.,* **110,** B08402, doi:10.1029/2004JB003251.

Suppe, J., 1981. Mechanic of mountain building and metamorphism in Taiwan, *Mem. Geol. Soc. China,* **4,** 67–89.

Suppe, J., 1984. Kinematics of arc-continent collision, flipping of subduction, and back-arc spreading near Taiwan, *Mem. Geol. Soc. China,* **6,** 21–33.

Tadokoro, K. & Ando M., 2002. Evidence for rapid fault healing derived from temporal changes in S wave splitting, *Geophys. Res. Lett.,* **29**(4), 1047, doi:10.1029/2001GK013644.

Tadokoro, K., Ando, M. & Umeda, Y., 1999. S wave splitting in the aftershock region of the 1995 Hyogo-ken Nanbu earthquake, *J. geophys. Res.* **104,** 981–992.

Tadokoro, K. *et al*. 2002. Monitoring of fault healing after the 1999 Kocaeli, Turkey, earthquake, *J. Seism.,* **6,** 411–417.

Tsai, Y.B., 1978. Plate subduction and the Plio-Pleistocene orogeny in Taiwan, *Petrol. Geol. Taiwan,* **15,** 1–10.

van der Lee, S. & Nolet, G., 1997. Upper mantle S velocity structure of North America, *J. geophys. Res.,* **102,** 22815–22838.

Vavryčuk, V., 1993. Crustal anisotropy from local observations of shear-wave splitting in West Bohemia, Czech Republic, *Bull. seism. Soc. Am.,* **83,** 1420–1441.

Wang, C.Y., Okaya, D.A., Ruppert, C., Davis, G.A., Guo, T.S., Zhong, Z. & Wenk, H.R., 1989. Seismic reflectivity of the Whipple Mountain shear zone in Southern California, *J. geophys. Res.,* **94,** 2989–3005.

Wu, F.T., Rau, R.J. & Salzberg, D., 1997. Taiwan orogeny: thin skin or lithospheric collision?, *Tectonophysics,* **274,** 191–220.

Yu, S.B., Chen, H.Y. & Kuo, L.C., 1997. Velocity field of GPS stations in the Taiwan area, *Tectonophysics,* **274,** 41–59.

Zinke, J.C. & Zoback, M.D., 2000. Structure-related and stress-induced shear-wave velocity anisotropy: observation from microearthquakes near the Calcaveras fault in central California, *Bull. seism. Soc. Am.* **90,** 1305–1312.